A Crystal Model for the Icosahedral Phase

WEIMIN BIAN† AND YIMEI ZHU*

Materials Science Division, Brookhaven National Laboratory, Upton, NY 11973, USA. E-mail: zhu@bnl.gov

Abstract

A crystal model is proposed that is in good agreement with the experimental electron diffraction patterns and high-resolution electron-microscopy images of the icosahedral phase in Mn–Al and related systems. Structurally, the model has long-range periodic translational order with a large unit cell (space group $Im\bar{3}$) containing 10 038 atoms as well as orientational order characterized by symmetry close to the $m\bar{3}\bar{5}$ point group. Such a periodic structure can explain the origin of the crystallographically forbidden icosahedral symmetries. The icosahedral phase may thus be considered as a complex cubic crystal.

1. Introduction

The first intermetallic phase with icosahedral symmetry was discovered by Shechtman, Blech, Gratias & Cahn (1984) in a rapidly solidified Al–14 at.%Mn alloy. This icosahedral phase exhibits diffraction spots as sharp as ordinary crystals but could not be indexed by any Bravais lattice (Shechtman *et al.*, 1984). Because the 'fivefold' symmetry associated with the icosahedral phase contravened the basic tenets of crystallography, the term 'quasicrystal' was coined to classify a phase that has long-range orientational order but no periodic translational order (Levine & Steinhardt, 1986). Later, phases with the same symmetry were found in various binary or ternary alloys (Dong, Hei, Wang, Song, Wu & Kuo, 1986; Ma & Stern, 1987; Hiraga, Lee, Hirabayashi, Tsai, Inoue & Masumoto, 1989) and even other classically forbidden symmetries, such as eightfold, tenfold and twelvefold phases, have been reported (Bendersky, 1985; Ishimasa, Nissen & Fukano, 1985; Wang, Chen & Kuo, 1987). Numerous models were developed to understand these unusual symmetries; for example, the icosahedral glass model (Shechtman & Blech, 1985), Penrose tiling models (Socolar & Steinhardt, 1986; Henley, 1986) and the random tiling model (Widom, Deng & Henley, 1989) and models using projections from six-dimensional space (Elser, 1985*a,b*). However, these models failed to explain all the experimental observations; in particular, they could not immediately render the real atomic distribution in three-dimensional physical space. Although models based on crystalline approximants were developed recently, the actual structures, however, were assumed to be aperiodic (Elser, 1985*a,b*; Poon, Dmowski, Egami, Shen & Shiflet, 1987; Zhang, Stroud, Libbert & Kelton, 1994).

Debates over the interpretation of diffraction data from the icosahedral phase, led by Linus Pauling (Pauling 1985, 1987, 1989), raised fundamental issues about the limits of our ability to distinguish between a true quasicrystal and a periodic crystal with complex large unit cells. Although Pauling suggested that a long-range, periodically and translationally ordered, twinned structure is responsible for the sharp Bragg reflections observed in the icosahedral phase, he did not present a convincing structural model. Motivated by Pauling's work, we investigated the icosahedral phase using advanced transmission-electron-microscopy and computer-simulation techniques. We found that the experimentally observed diffraction patterns as well as high-resolution electron-microscopy (HREM) images of the icosahedral phase can be well explained by a crystal structure having a strict translational periodicity, being composed of many interpenetrating dodecahedrons and icosahedrons.

2. Crystal model

The unit cell of the crystal model we propose for Al–14 at.%Mn has a body-centered cubic (b.c.c.) structure belonging to the $Im\bar{3}$ space group with a cube edge of 5.4 nm. The structure can be described in terms of dodecahedrons and icosahedrons with three different length scales. The basis of the b.c.c. lattice is the large dodecahedron. One large dodecahedron surrounds the center of the unit cell and eight equivalent dodecahedrons surround the corner of the cube [2(a) Wyckoff positions]. At each of the 20 corners of the large dodecahedrons are located medium-sized icosahedrons, and at the corners of the icosahedrons are the centers of the small dodecahedrons. All the dodecahedrons and icosahedrons have the same orientations. The unit cell we propose is built in such a manner and has a total of 10 038 atoms (1405 Mn and 8633 Al), which yield a crystal density of 3.27 g cm^{-3}, being very close to the value of 3.26 (6) g cm^{-3} measured experimentally (Chen, Chen, Inoue & Krause, 1985). The shortest atomic distance within the small dodecahedron is about 3.0 Å, similar to

---

† On leave from Materials Testing Center, Northeastern University, Shenyang, China.

Table 1. *Wyckoff position of the clusters in the proposed model for the icosahedral phase*

$a = 5.4$ nm, space group $Im\bar{3}$ (no. 204), calculated density: 3.27 g cm^{-3}.

Wyckoff position	x	y	z	Wyckoff position	x	y	z
2(*a*)	0	0	0	24(*g*)	0	0.191	0.264
12(*e*)	0.309	0	0.500	24(*g*)	0	0.382	0.382
16(*f*)	0.191	0.191	0.191	24(*g*)	0	0.427	0.500
12(*d*)	0.382	0	0	48(*h*)	0.309	0.309	0.073
16(*f*)	0.118	0.118	0.118	48(*h*)	0.309	0.073	0.073
24(*g*)	0	0.191	0.118	48(*h*)	0.118	0.382	0.427
24(*g*)	0	0.073	0.191	48(*h*)	0.382	0.118	0.309
24(*g*)	0	0.427	0.118	48(*h*)	0.382	0.073	0.191
24(*g*)	0	0.264	0.309				

the diameters of the Mn and Al atoms. Fig. 1 shows the $\langle 001 \rangle$ projection of the unit cell, where the big circles represent the corner sites of the big dodecahedrons [12(*e*) and 16(*f*) Wyckoff positions], the small ones represent the corner sites of the medium icosahedrons [12(*d*), 16(*f*), 24(*g*) and 48(*h*) Wyckoff positions] and only those dodecahedrons and icosahedrons projecting into the center of the unit cell are drawn. For simplicity and clarity, we did not include the small dodecahedrons. Thus, the unit cell shown in Fig. 1 can be considered as a cell where each position actually is occupied by the small dodecahedrons, or a 21-atom cluster (the individual column of atoms within the cluster in the major zone axes cannot be resolved by HREM). Such a unit cell consists of 478 clusters; Table 1 lists their Wyckoff positions.
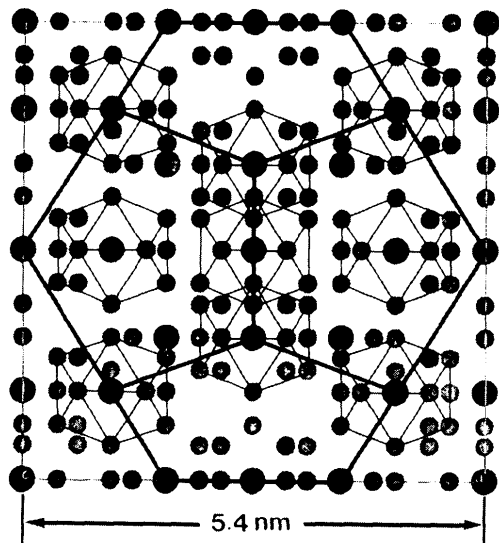

Fig. 1. The $\langle 001 \rangle$ projection of the unit cell; only those dodecahedrons and icosahedrons projecting into the center of the cell are depicted. Either the big circle (at the corner positions of the big dodecahedron) or the small circle (at the corner positions of the medium icosahedrons) represent a 21-atom cluster (or a small dodecahedron). There are 478 clusters and their Wyckoff positions are listed in Table 1.

3. Results and discussion

We calculated the diffraction patterns and high-resolution images of our model and compared them with the experimental observations. Figs. 2(*a*)–(*c*) show, respectively, the selected-area diffraction (SAD) patterns of the so-called twofold, threefold and fivefold axes observed in rapidly quenched Al–14 at.%Mn. Figs. 2(*d*)–(*f*) are the corresponding SAD patterns calculated using kinematical diffraction theory (sample thickness 150 nm and incident electron energy 200 keV). The main features of these simulated patterns agree well with the experimental ones except for the intensity of a few reflections and the lack of several weak spots (both of which can be attributed to dynamical effects, including double diffractions). Since the simulation was based on a periodic structure, we can easily index all diffraction spots in terms of three Miller indices. Analysis of these indices suggests that each SAD pattern did not result from a single zone-axis diffraction but from several closely oriented zone axes. For example, the SAD pattern of Fig. 2(*f*) was generated by the superposition of the [305], [508] and [8,0,13], ... axes; the rotation angles from the [001] axis to each axis are 30.96, 32.01 and 31.61°, respectively. All are very close to 31.71°, which is the angle between a twofold and a fivefold axis in the $m\bar{3}5$ point group assigned for quasicrystals (Fig. 3*a*). In a conventional electron diffraction experiment, if the [001] axis of the crystal is rotated 31.71° around the [010] axis, these three zone axes simultaneously satisfy the Bragg conditions and cannot be separated. Such superposition in the projected diffraction pattern, especially when the unit cell is large, can yield a pseudo-fivefold symmetry that is indistinguishable from true fivefold symmetry (point group $m\bar{3}5$) in SAD.

Similar pseudo-symmetries were found in Fig. 2(*d*) (twofold) and Fig. 2(*e*) (threefold), which were attributed to the reflections from $\langle 358 \rangle$, $\langle 15,25,39 \rangle$, $\langle 31,49,79 \rangle$, ... and $\langle 038 \rangle$, $\langle 0,5,13 \rangle$, $\langle 0,8,21 \rangle$, ... zone axes, respectively. To describe the superposition of SAD patterns, we now use N-$\langle uvw \rangle$ to represent a zone family consisting of several *nearly* parallel zone axes, where $\langle uvw \rangle$ is the lowest-index zone in the family (*e.g.* for a family of $\langle 038 \rangle$, $\langle 0,5,13 \rangle$, $\langle 0,8,21 \rangle$, ..., $\langle uvw \rangle = \langle 038 \rangle$). Thus, the SAD patterns shown in Figs. 2(*d*)–(*f*) can be defined as the N-$\langle 358 \rangle$, N-$\langle 038 \rangle$ and N-$\langle 305 \rangle$ axes, respectively. We also found that in $m\bar{3}$ the SAD pattern of the $\langle 001 \rangle$ axis (Fig. 2*g*) is almost identical to that of the N-$\langle 358 \rangle$ axis (Fig. 2*d*), while the $\langle 111 \rangle$ (Fig. 2*h*) is almost identical to the N-$\langle 038 \rangle$ (Fig. 2*e*). The rotation angles between these pseudo-twofold, -threefold and -fivefold axes (Fig. 3*b*) are so close to those between the true twofold, threefold, and fivefold ones in $m\bar{3}5$ (see Table 2) that they could not be distinguished in SAD patterns. In $m\bar{3}$, there are only six N-$\langle h0l \rangle$ axes and twelve N-$\langle hkl \rangle$ because this symmetry group does not have a fourfold rotation symmetry. Thus, we conclude that the six 'fivefold' axes reported for the icosahedral phase

($m\bar{3}\bar{5}$) are actually six N-$\langle 305 \rangle$ axes (pseudo-fivefold) in $m\bar{3}$. The ten 'threefold' axes are six N-$\langle 038 \rangle$ (pseudo-threefold) and four $\langle 111 \rangle$ (true threefold) axes and the fifteen 'twofold' are twelve N-$\langle 538 \rangle$ (pseudo-twofold) and three $\langle 001 \rangle$ (true twofold) axes. Fig. 3 compares the true and pseudo-fivefold, -threefold, and -twofold axes in stereographic projection between the $m\bar{3}\bar{5}$ and $m\bar{3}$ point groups.

The key issue is whether the icosahedral phase has a true fivefold axis that is forbidden in conventional crystallography. Using convergent-beam electron diffraction (CBED), we carefully examined many Mn–Al samples in the zone axes that appear to be fivefold in SAD, but never observed any samples with a true fivefold symmetry. Fig. 2(i) shows the CBED pattern from the same zone axis as Fig. 2(c); although the position of the diffraction discs appears to be fivefold, the exact overall symmetry of their intensities is twofold nonetheless. The broken symmetry is most visible from the Kikuchi bands, which only exhibit a mirror symmetry in the $\langle 001 \rangle$ direction, consistent with our model. This observation also is consistent with the CBED study by Tanaka
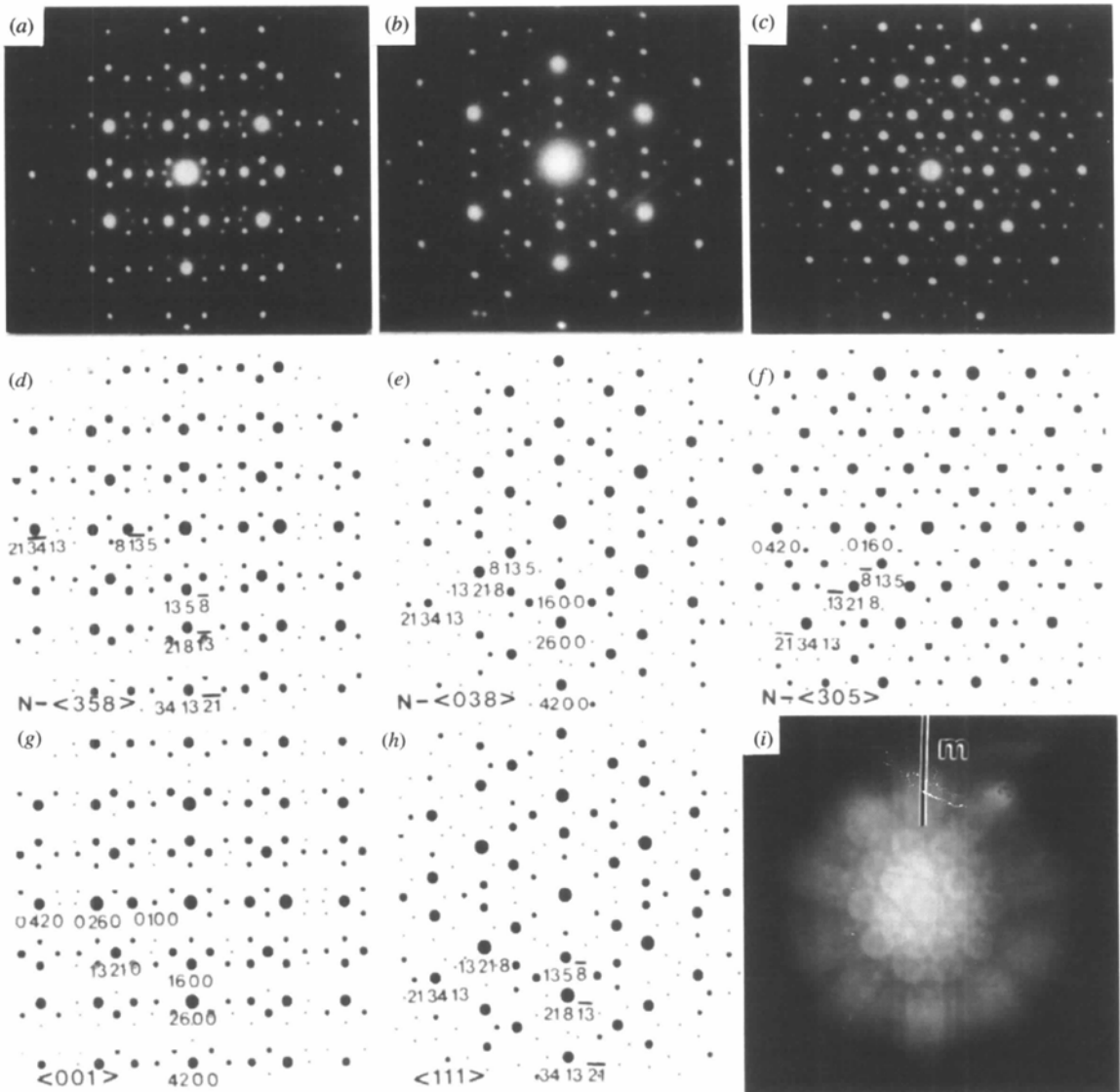

Fig. 2. (a)–(c) SAD patterns observed in rapidly quenched Al–14 at.%Mn alloy. (a) Pseudo-twofold, (b) pseudo-threefold [tilted 20.9° from (a)], and (c) pseudo-fivefold [tilted 31.7° from (a)]. (d)–(h) are the calculated diffraction patterns using the proposed model. (d) The N-$\langle 358 \rangle$ axis, (e) the N-$\langle 038 \rangle$ axis, (f) the N-$\langle 305 \rangle$ axis, (g) the $\langle 001 \rangle$ axis [identical to the N-$\langle 358 \rangle$ axis (d)], and (h) the $\langle 111 \rangle$ axis [identical to the N-$\langle 038 \rangle$ axis (e)]. The simulated patterns match well with the observed ones and all the diffraction spots were indexed with standard Miller indices. (i) Observed CBED pattern along the pseudo-fivefold axis from the same area of (c). The Kikuchi bands show clearly that there is only one mirror symmetry.

& Terauchi (1985), who could not find any true fivefold axis in the alloy. Our study unambiguously showed that there is no true fivefold axis in the icosahedral phase, and the symmetries in SAD of the icosahedral phase can therefore be explained by a Bravais lattice.

Another argument in favor of the quasicrystal concept is that the observed ratio of d spacing of two 'consecutive' reflections of the icosahedral phase appeared to be not rational [close to the golden ratio $\tau = (1 + 5^{1/2})/2 \simeq 1.618$], e.g. the reflections in the $\langle h00 \rangle$ systematic rows

(a)

⊕ pseudo $\bar{5}$-axis   ▲ pseudo $\bar{3}$-axis   ⊘ pseudo 2-axis

(b)

Fig. 3. Stereographic projections of the symmetry elements of the icosahedral phase: (a) the $m\bar{3}\bar{5}$ point group used in the literature for the icosahedral phase, and (b) the $m\bar{3}$ point group from the present model. Only three $\langle 001 \rangle$ axes and four $\langle 111 \rangle$ axes show the same symmetry in (a) and (b). Note that the orientations of the $\langle 358 \rangle$, $\langle 038 \rangle$ and $\langle 305 \rangle$ axes in (b) are identical to those of the twofold, threefold and fivefold axes in (a), respectively.

in Figs. 2(e) and (f). Apparently, the irrational value gives the impression that the structure does not have strict translational periodicity. To understand the intensity distribution, we examined the structure factors for all reflections of the $\langle h00 \rangle$ systematic row and found that they closely follow the extinction rule of the $Im\bar{3}$ space group, i.e. no reflections are allowed when $h = 2n + 1$. Although the strong reflections are 10,0,0, 16,0,0, 26,0,0, ..., other reflections ($h = 2n$) exist but have much smaller structure factors. Similar characteristics were observed for the $\langle 358 \rangle$ systematic rows (i.e. strong intensity for 358, 5,8,13, 8,13,21, ...) and were only found in the true and pseudo-twofold directions. Such intensity distribution is not unusual and can be easily attributed to the icosahedral clusters located inside the unit cells of the cubic crystal (Pauling, 1985).

The sharpness of the diffraction spots in patterns of fivefold symmetry has puzzled the crystallographic community since the discovery of quasicrystals. According to classical diffraction theory, the perfection or the translational periodicity of a sufficiently large crystal gives rise to sharp diffraction peaks, while the imperfections of a crystal, such as stacking faults and dislocations, cause peak broadening. In contradiction, Stephens & Goldman (1986) showed that clusters of atoms densely packed and complying with specific rules that enforce long-range icosahedral bond-orientational order also might generate sharp diffraction maxima. What is common between our approach and theirs is that both deal with clusters of fivefold symmetry. However, we have abandoned the assumption of aperiodicity, rather, we show that crystals obeying the symmetry rules of classical crystallography may result in intensity distribution of Bragg reflections in reciprocal space with approximately fivefold symmetry.

Our structural model also agrees with the observations of HREM. In fact, for most of the published high-quality HREM images of the icosahedral phase and related systems (including Al–Mn–Si, Al–Cu–Fe, Al–Ru–Cu alloys), we have found unit cells with a periodicity of about 5 nm in these images (Hiraga, 1987, 1991; Hiraga et al., 1989; Hiraga, Zhang, Hirabayashi, Inoue & Masumoto, 1988; Kan, Robertson, Moss, Kukik, Ishimasa, Mori, Quivy, Gratias, Elser & Zschack, 1993), especially in the regions where few planar defects were present. The size of the unit cell is very close to that found in high-resolution X-ray diffraction and calculated using large-cell projection (Goldman & Kelton, 1993). Fig. 4 shows a HREM image recorded along the pseudo-fivefold axis of the Al–Cu–Fe alloy. The dot pattern is a potential map of the local crystal structure. The periodicity of the image along the [010] and the [503] directions (~5.0 and 6.9 nm, respectively) is clearly visible (marked as two sets of parallel white lines in Fig. 4). The inset is the calculated unit-cell projection along the N-[305] zone axis (the Wyckoff positions of the unit cell are shown in Table 1), showing very good
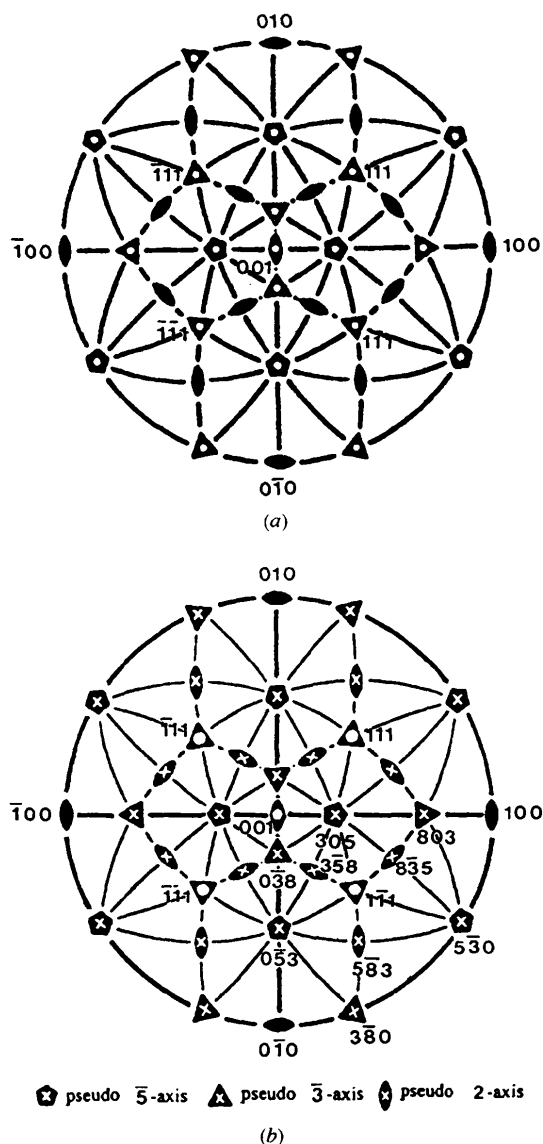
Table 2. *The rotation angles (°) between the true and pseudo-twofold, -threefold and -fivefold axes in m$\bar{3}\bar{5}$ and m$\bar{3}$ point groups*

Owing to the equivalent operations, there are many equivalent rotations between these zone axes, so only the smallest angles are listed here.

	m$\bar{3}\bar{5}$ twofold	m$\bar{3}$ N-(358)	m$\bar{3}\bar{5}$ threefold	m$\bar{3}$ N-(038)	m$\bar{3}\bar{5}$ fivefold	m$\bar{3}$ N-(305)
m$\bar{3}\bar{5}$ twofold	36.0		20.92		31.71	
m$\bar{3}$ (001)		36.09		20.56		30.96
m$\bar{3}$ N-(358)		36.28		20.93		31.91
m$\bar{3}\bar{5}$ threefold	20.91		41.82		37.38	
m$\bar{3}$ (111)		21.07		41.99		37.62
m$\bar{3}$ N-(308)		20.93		41.22		36.59
m$\bar{3}\bar{5}$ fivefold	31.71		37.38		63.43	
m$\bar{3}$ N-(305)		31.91		36.59		63.82

agreement with the experimental one. Here, each dot does not represent a single atom column but the projection of a cluster that involves ten equally spaced nearest neighbors (spacing ~ 0.18 nm) from the projected small dodecahedron (the atom columns within the cluster are not resolved). The same calculated unit cell can also be matched to the HREM structural image of Si-doped Mn–Al reported by Hiraga (1987).

In discussing the detailed structure of the icosahedral phase, we have to bear in mind that the dodecahedron and the icosahedron have the same crystallographic symmetry. Although the model we present here is based on interpenetrating dodecahedrons and icosahedrons (this was a process of trial and error: we choose all the dodecahedrons and icosahedrons to align in the same orientations and the ratio of their length scales close to τ), other models may also generate diffraction patterns and high-resolution images that match the experimental observations. One of the criteria in choosing a correct model may be related to the size of the unit cell and the total number of the atoms it contains, *i.e.* the density of the material. Imperfect dodecahedrons and/or icosahedrons can be introduced in modeling because these may be produced by the rapid solidification process
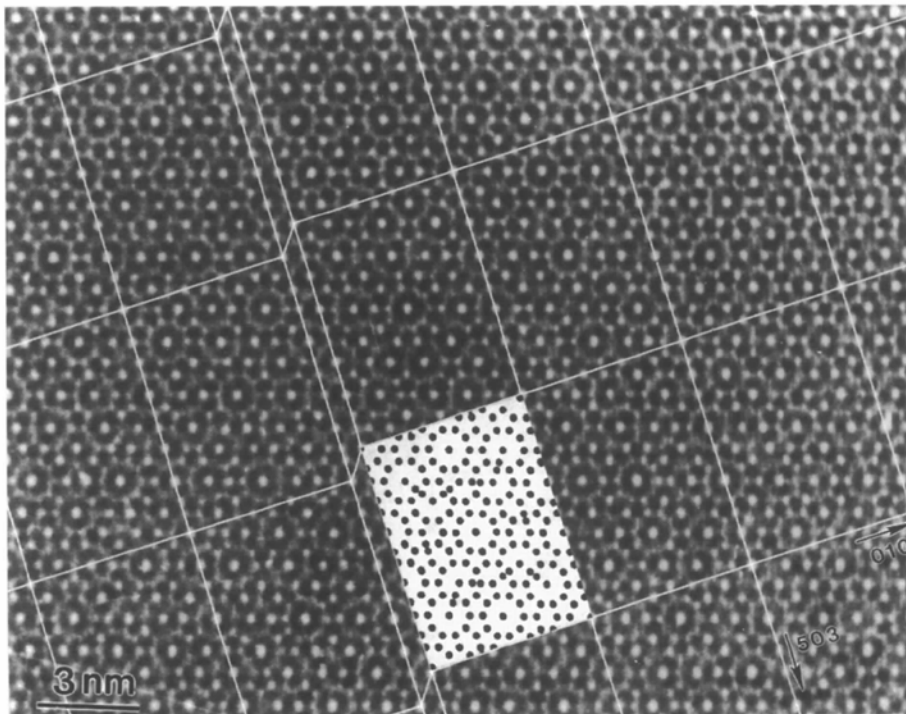

Fig. 4. HREM image along the pseudo-fivefold axis showing a potential map of the local structure in Al–Cu–Fe (defocus value -60 nm). Each white dot corresponds to the projection of one cluster. Inset is the N-(305) projection of the unit cell of the proposed model; it is in agreement with the experimental image. The periodic translational order in [010] and [503] directions is marked by the parallel white lines. Note that there is a planar defect that yields a lattice displacement in the area.

under which the alloys were formed. Little difference would be noted in both calculated zone-axis diffraction patterns and projected high-resolution images if clusters or atoms at certain Wyckoff positions were removed.

4. Conclusions

Using simulations of electron diffraction and high-resolution structural images, we have demonstrated that the quasicrystal of the icosahedral phase can be described as a complex b.c.c. crystal. The crystal has a large unit cell containing more than 10 000 atoms. It does not have true fivefold symmetry, although its SAD pattern has fivefold appearance. Such pseudo-symmetry originates from the superposition of reflections from several nearly parallel zone axes. Since the icosahedral phase is modeled as a crystal with periodic translational order, the sharpness and the symmetry of its diffraction peaks can be explained in the framework of classical diffraction theory.

References

Bendersky, L. (1985). *Phys. Rev. Lett.* **55**, 1461–1463.
Chen, H. S., Chen, C. H., Inoue, A. & Krause, J. T. (1985). *Phys. Rev. B*, **32**, 1940–1944.
Dong, C., Hei, Z. K., Wang, L. B., Song, Q. H., Wu, Y. K. & Kuo, K. H. (1986). *Scr. Metall.* **20**, 1155–1158
Elser, V. (1985*a*). *Phys. Rev. B*, **32**, 4892–4898.
Elser, V. (1985*b*). *Phys. Rev. Lett.* **54**, 1730.
Goldman, A. I. & Kelton, R. F. (1993). *Rev. Mod. Phys.*, **65**, 213–230.
Henley, C. L. (1986). *Phys. Rev. B*, **34**, 797–816.
Hiraga, K. (1987). *J. Microsc.* **146**, 245–260.
Hiraga, K. (1991). *Quasicrystals: the State of the Art*, edited by D. P. Divincenzo & P. Steinhardt, pp. 95–110, Figs. 1, 5, 9. Singapore: World Scientific.
Hiraga, K., Lee, K. H., Hirabayashi, M., Tsai, A. P., Inoue, A. & Masumoto, T. (1989). *Jpn. J. Appl. Phys.* **28**, L1624–L1627.
Hiraga, K., Zhang, B. P., Hirabayashi, M., Inoue, A. & Masumoto, T. (1988). *Jpn. J. Appl. Phys.* **27**, L951–L953.
Ishimasa, T., Nissen, H. U. & Fukano, Y. (1985). *Phys. Rev. Lett.* **55**, 511–513.
Kan, X. B., Robertson, J. L., Moss, S. C., Kukik, J., Ishimasa, T., Mori, M., Quivy, A., Gratias, D., Elser, V. & Zschack, P. (1993). *J. Non-cryst. Solids*, **153&154**, 33–39.
Levine, D. & Steinhardt, P. J. (1986). *Phys. Rev. B*, **34**, 596–616.
Ma, Y. J. & Stern, E. A. (1987). *Phys. Rev. Lett.* **58**, 1956–1959.
Pauling, L. (1985). *Nature (London)*, **317**, 512–514.
Pauling, L. (1987). *Phys. Rev. Lett.* **58**, 365–368.
Pauling, L. (1989). *Proc. Natl Acad. Sci. USA*, **86**, 8595–8599.
Poon, S. J., Dmowski, W., Egami, T., Shen, Y. & Shiflet, G. J. (1987). *Philos. Mag. Lett.* **56**, 259–264.
Shechtman, D. & Blech, I. A. (1985). *Metall. Trans.* A**16**, 1005–1012.
Shechtman, D., Blech, I., Gratias, D. & Cahn, J. W. (1984). *Phys. Rev. Lett.* **53**, 1951–1953.
Socolar, J. E. S. & Steinhardt, P. J. (1986). *Phys. Rev. B*, **34**, 617–647.
Stephens, P. W. & Goldman, A. I. (1986). *Phys. Rev. Lett.* **56**, 1168–1171.
Tanaka, M. & Terauchi, M. (1985). *Ultramicroscopy*, **17**, 279–286.
Wang, N., Chen, H. & Kuo, K. H. (1987). *Phys. Rev. Lett.* **59**, 1010–1013.
Widom, M., Deng, D. P. & Henley, C. L. (1989). *Phys. Rev. Lett.* **63**, 310–313.
Zhang, X., Stroud, R. M., Libbert, J. L. & Kelton, K. F. (1994). *Philos. Mag. B*, **70**, 927–950.